

Extending Scattering-Parameter Approach to Characterization of Linear Time-Varying Microwave Devices

Kenton Green, *Member, IEEE*, and Roman Sobolewski, *Member, IEEE*

Abstract—In this paper, we apply the theory of linear time-varying differential systems of equations to defining an extension of the standard scattering parameters. This extended parameter $\tilde{S}(\omega, t)$ is a function of both time and frequency. With this definition, we can accurately characterize rapidly time- and frequency-varying linear lumped causal microwave devices, in particular, photoconductive microwave switches. We discuss the similarities between $\tilde{S}(\omega, t)$ and the standard S -parameter approach and describe a measurement technique. We also derive some important properties of the $\tilde{S}(\omega, t)$ -parameters and describe conditions under which microwave devices such as photoconductive switches can be analyzed by this technique. To demonstrate the usefulness of $\tilde{S}(\omega, t)$, we derive the complete transfer function of the time-varying lumped-element model of a photoconductive switch. We also show the limitations of conventional time-invariant assumptions (based on windowing or apodization) to accurately model linear time-varying devices.

Index Terms—Ambiguity function, generalized projections, linear frequency time varying, optoelectronic, phase retrieval, photoconductive, S -matrix scattering parameter, time–frequency distribution, transient frequency response.

I. INTRODUCTION

A COMMON method of characterizing the frequency response of microwave devices is to assume a linear time-invariant (LTI) microwave filter model and apply measurement tools such as S -parameters. If the device has significant temporal response, the most convenient model is a linear-frequency invariant (LFI) modulator model. Table I presents the canonical transfer functions of the two ideal shift-invariant microwave devices in each of the two domains—time and frequency—to emphasize their complementary nature. All dependent variables are complex; t and τ are in seconds; ω and ξ are in radians per second; $a(\omega)$ and $b(\omega)$ are the conventional S -parameter power waves, and $A(t)$ and $B(t)$ are their respective Fourier transforms; $S(\omega)$ and $h(t)$ are the LTI scattering parameter and its Fourier transform (the impulse response); $k(t)$ and $K(\omega)$ are the

TABLE I
COMPARISON OF THE TRANSFER FUNCTIONS OF LTI FILTERS AND LFI MODULATORS

Domain	LTI filter	LFI modulator
Time	$B_i(t) = \int_{-\infty}^{\infty} h_{ij}(t-\tau) A_j(\tau) d\tau$	$B_i(t) = k_{ij}(t) \cdot A_j(t)$
Frequency	$b_i(\omega) = S_{ij}(\omega) \cdot a_j(\omega)$	$b_i(\omega) = \int_{-\infty}^{\infty} K_{ij}(\omega-\xi) a_j(\xi) d\xi$

LFI modulation parameter and its Fourier transform. The subscripts refer to the ports of the device. We use analytic (complex), not real signals. The route we will use to define \tilde{S} is motivated by the observation that, in the relationships for filters and modulators presented in Table I, the roles of time and frequency are complementary, i.e., the one-dimensional (1-D) characterization functions are along orthogonal axes in the complex plane. Thus, we realize that a more general two-dimensional (2-D) characterization is possible by considering the device's response over the entire plane.

To characterize devices in more complicated operating regimes, various analysis and synthesis techniques—such as complex frequency-hopping [1] and “transient” S -parameters—have been developed. Their application extends the concept of transfer functions to exponential transmission lines [2], nonuniformly coupled transmission lines [3], transmission lines with time-varying [4] or nonlinear loads [5], [6], or some combination of these [7]–[9].

The functional form of the S -parameter extension described in this paper will be identified as $\tilde{S}(\omega, t)$ and is distinct from the above-mentioned methods because it allows complete characterization of linear time-varying microwave devices. Linear time-varying devices are those whose transmission and reflection are both time and frequency varying (i.e., not shift invariant on either the time or frequency axis). The time variations (modulation) and frequency variations (filtering) are “rapid” (of the order of the signal's carrier cycle and spectral widths, respectively). A linear device that is not shift invariant along either axis can be considered a time-varying filter with different impulse responses at each moment in time, or equivalently a modulator with finite frequency response that modulates each frequency differently.

Microwave devices whose properties are controlled by an optical signal have been described in [10] and [11]. These devices should be modeled as linear time-varying lumped- or distributed-element devices when the electrical and optical input

Manuscript received June 22, 1999. This work was supported by the U.S. Department of Energy Office of Inertial Confinement Fusion under Cooperative Agreement DE-FC03-92SF19460 and by the University of Rochester. The work of K. Green was supported by the Frank Horton Graduate Fellowship Program.

K. Green is with the Laboratory for Laser Energetics, Department of Electrical and Computer Engineering, University of Rochester, Rochester NY 14623-1299 USA.

R. Sobolewski is with the Laboratory for Laser Energetics, Department of Electrical and Computer Engineering, University of Rochester, Rochester NY 14623-1299 USA and also with the Institute of Physics, Polish Academy of Sciences, PL-02668 Warszawa, Poland.

Publisher Item Identifier S 0018-9480(00)08732-9.

signals are isolated, and charge-carrier population dynamics are on the time scale of the electrical signal [12]–[15]. If the change in the value of the time-varying element is rapid enough, conventional (windowed) S -parameter techniques will time- and/or frequency-average the variations, producing an inaccurate result that is dependent on the specifics of the windowing function.

Linear time-varying devices (filters) are well established in the signal-processing [16], [17], communication [18], and automatic-control [19] fields; however, in the microwave regime, they have not been necessary since the variation of microwave filter properties is typically caused either by slowly varying (mechanical) effects or by rapid (nonlinear) transitions between steady-state regimes (e.g., microwave diode switches or mixers). For these types of devices, windowing provides adequate solutions. The motivation of our analysis is to introduce a characterization technique that is a superset of the S -parameters and is applicable to devices (such as photoconductive microwave switches) that are linear filters with rapid modulation of amplitude and/or phase. For such devices, the use of conventional methods of linear microwave circuit characterization (e.g., spectrum and network analyzers), based on windowing and application of Fourier transforms and the convolution integral, can lead to incorrect characterization results.

Motivated by these limitations, we combine the complementary 1-D LTI and LFI transfer functions into a single 2-D transfer (or system) function, calling it $\tilde{S}(\omega, t)$ to suggest its relationship to the conventional $S(\omega)$ -parameters. The synthesis of this 2-D \tilde{S} -parameter requires more extensive signal application and measurement than conventional S -parameters. However, it is possible to simplify the measurement process by using the theory of generalized projections, as used in 2-D phase retrieval, taking advantage of the 2-D nature of \tilde{S} . This allows for the reconstruction of the full vector (complex) 2-D transfer function from magnitude-only measurements. This method applies to practical microwave devices where the transfer function is zero outside some finite temporal and spectral window, i.e., if it has known compact support along both axes [20].

$\tilde{S}(\omega, t)$ can be measured in either the “frequency domain” or the “time domain.” In the frequency-domain approach, a single-frequency input wave is applied to the device-under-test (DUT) for the time duration of interest. The temporal evolution of the output signal’s amplitude and phase versus a reference is then recorded. To separate the device’s effect on signal amplitude and phase, the analytic signal is measured by reapplying the input wave, shifted by $\pi/4$. This requires that the time-varying device be deterministic and triggerable. By applying signals at a range of frequencies over a given time span, a “map” of $\tilde{S}(\omega, t)$ is constructed of time slices at each successive frequency. In the time-domain approach, a series of impulse functions is applied at time intervals over the period of interest. The impulse response of the system to each successive impulse is then recorded. In this way, $\tilde{S}(\omega, t)$ is constructed of frequency slices at each time interval.

Although these measurement descriptions are intuitively appealing, it may not be readily apparent how to extract an input–output relationship such as $\tilde{S}(\omega, t)$ from the measured

signals, create a device model, and apply it to the calculation of output signals given an arbitrary input signal. In Section II, we state the definition of the extended scattering parameter \tilde{S} . In Section III, we apply \tilde{S} -parameters to device analysis by considering a lumped-element example model. We synthesize the device’s transfer function both from its \tilde{S} -parameter definition and directly from the differential equations. We then compare output signals that result from applying \tilde{S} to those obtained by windowing. By so doing, we demonstrate the limitations of the windowing technique. Finally, in Section IV, we present conclusions and link our model to the experimental characterization of a photoconductive microwave device used in an optoelectronic pulse-shaping system, which we will present in detail in another paper.

II. MATHEMATICAL FORMULATION

The time-domain differential equation describing a linear lumped-element device with time-variable coefficients is

$$\alpha_0(t) \frac{d^n}{dt^n} B_i(t) + \alpha_1(t) \frac{d^{n-1}}{dt^{n-1}} B_i(t) + \cdots + \alpha_n(t) B_i(t) = \mathcal{L}_{ij}(p, t) B_i(t) = A_j(t) \quad (1)$$

where the coefficients α are determined by the (time-varying) dependencies between the nodes of the circuit (e.g., the lumped-element models of resistance, capacitance, and inductance). The ports of the device described by the circuit model are a subset of the nodes of the circuit model. The signals $A(t)$ and $B(t)$ in (1) are defined in Table I. Also, we have used the operator notation $\mathcal{L}(p) = \alpha_0 p^n + \alpha_1 p^{n-1} + \cdots + \alpha_n$, where p is the differential operator d/dt [20]. Note that the derivation is being done for a device with a finite number of nodes and, therefore, a finite number of (time-varying) poles and zeros. A more-general derivation can show that $\tilde{S}(\omega, t)$, like $S(\omega)$, is applicable to distributed-element devices.

For an LTI model, there is no time variation in the coefficients of (1); it, therefore, simplifies to

$$\mathcal{L}_{ij}(p) B_i(t) = A_j(t). \quad (2)$$

Assuming complex exponentials $e^{\pm j\omega t}$ for the basis function solutions (which simplifies the differential operator p to ω) and converting to S -parameter notation $S_{ji}(\omega) = \mathcal{L}_{ij}^{-1}(p)$, we derive the frequency-domain filter transfer function of Table I. These Fourier transforms are useful for microwave device characterization because they transform between a system of differential equations and a system of algebraic equations; i.e., they are “compatible” integral transform operators [21]. Noncompatible transforms result in relationships between the input and output that are not generally algebraic. In contrast to modulators and filters, a compatible integral transform operator for a general linear device depends on the functional form of the variable coefficients in (1). This means that the basis functions that result in algebraic relationships are not, in general, $e^{\pm j\omega t}$, but are dependent on the particular form of modulation and frequency response.

The key to the modeling technique described in this paper is that to remain independent of the specifics of the temporal variations in device properties, we choose a noncompatible trans-

form that will enable us to continue to use $e^{\pm j\omega t}$ basis functions. Several important implications of this choice will be mentioned during our derivation of the properties of the system function. To define the transfer function for a linear lumped- or distributed-element device, we will drop the assumptions of time and frequency invariance. The resulting equation (in the time domain) can be written as

$$\tilde{S}_{ij}(\omega, t) = \left. \frac{B_i(t)}{A_j(t)} \right|_{A_j(t)=e^{j\omega t}} \quad (3)$$

which differs from the traditional S -parameter definition in that it is now a function of both time and frequency. From (1), $\tilde{S}_{ij}(\omega, t) = L_{ij}^{-1}(p, t)$, where the differential operator p simplifies to ω . Equation (3) states that the output signal $B_i(t)$ has time-varying amplitude and phase modulation for each input sine wave $A_j(t)$ (as with a modulator), but in addition, this modulation is generally different for each frequency of $A_j(t)$ (as with a filter).

By virtue of the linearity of the device, superposition applies and $B_i(t)$ can be defined in terms of $A_j(\tau)$ according to

$$B_i(t) = \int_{t_0}^t \tilde{h}_{ij}(\tau, t) A_j(\tau) d\tau. \quad (4)$$

where the limits of the integral have been set by assuming causality and that the signal is zero at times before the trigger. Equation (4) is a generalization of the time-invariant convolution in Table I with the impulse response function being now the more-general Green's function $\tilde{h}(\tau, t)$, i.e., it now depends separately on impulse time τ and observation t and not merely on the difference. From (3) and (4), $B_i(t) = \tilde{S}_{ij}(\omega, t)e^{j\omega t}$ is the output of the device for an input $A_j(t) = e^{j\omega t}$, given that the (variable) coefficients evolve deterministically from time $t = t_0$.

Substituting (4) into (3) results in a transform relationship between the system function \tilde{S} and the new generalized impulse response \tilde{h}

$$\tilde{S}_{ij}(\omega, t) = \int_{-\infty}^{\infty} \tilde{h}_{ij}(\tau, t) e^{-j\omega(t-\tau)} d\tau. \quad (5)$$

The two transfer functions $\tilde{S}_{ij}(\omega, t)$ and $\tilde{h}_{ij}(\tau, t)$ are related by a Fourier transform of the first axis. In addition to these two transfer function definitions, two other definitions result from transforming \tilde{S} and \tilde{h} in each of their second variables. The resulting input–output relationships for these four system functions are listed in Table II.

An important distinction exists between these 2-D transfer functions and ambiguity functions (also called time–frequency representations) that are found by windowing signals: 2-D transfer functions represent device responses, while ambiguity functions represent 1-D signals. The former may have arbitrarily sharp features (peaks and valleys) on either (independent) axis, whereas the windowed function has an inverse relationship between the (dependent) axes. This inverse relationship for windowed signals is due to the uncertainty principle: a narrow windowing of a signal in time (to prevent averaging the time fluctuations of the system) necessarily implies a widening of the spectral window (which forces

TABLE II
INPUT–OUTPUT RELATIONSHIPS FOR ALL FOUR 2-D SYSTEM FUNCTIONS

Domain	Input time	Input frequency
Output time	$B_i(t) = \int_0^t \tilde{h}_{ij}(\tau, t) A_j(\tau) d\tau$	$B_i(t) = \int \tilde{S}_{ij}(\omega, t) a_j(\omega) e^{j\omega t} d\omega$
Output frequency	$b_i(\omega) = \int \tilde{k}_{ij}(t, \omega) A_j(t) e^{-j\omega t} dt$	$b_i(\omega) = \int_0^{\infty} \tilde{K}_{ij}(\xi, \omega) a_j(\xi) d\xi$

averaging over spectral fluctuations) and vice versa [22]–[25]. Thus, windowing cannot measure sharply varying 2-D transfer functions, as shown in Section I.

From (4), we get a relationship between input and output by replacing $A_j(\tau)$ with its transform $\int a_j(\omega) e^{j\omega\tau} d\omega$, inverting the order of integration and substituting from (5)

$$B_i(t) = \tilde{\mathcal{F}}^{-1} \left[\tilde{S}_{ij}(\omega, t) a_j(\omega) \right] \quad (6)$$

where the differential transform operator $\tilde{\mathcal{F}}^{-1}$ is *similar* to the inverse Fourier transform, but with the variable t held as a constant parameter. Equation (6) is analogous to the frequency-domain filter relation in Table I in that the signal is the transform of the product of the scattering parameter and the input spectral function. Unlike conventional Fourier transforms, however, (4) is not a convolution, and the argument inside the brackets of (6) is not the product of the two 1-D functions. This means that, in general, as mentioned earlier, there is no algebraic relationship between the input and output

$$b_i(\omega) \neq \tilde{S}_{ij}(\omega, t) a_j(\omega). \quad (7)$$

The function $\tilde{S}(\omega, t)$ cannot be found by taking a quotient $b(\omega)/a(\omega)$, as can be done for $S(\omega)$ of LTI devices. For network synthesis, where a model (differential equation) must be synthesized from a given (measured) $\tilde{S}(\omega, t)$, this consequence of noncompatible transforms has no major negative implications; in fact, choosing the noncompatible (but Fourier-like) transform allows the use of standard Fourier transform tables, making the synthesis easier. On the other hand, for network analysis, where the output $B(t)$ is to be found in terms of $A(t)$, the significance of (7) is that only simple linear time- and frequency-varying device models (which can be solved directly, with only first- or second-order differential equations) can be created since signal flow graphs and the combination of series and parallel devices are no longer algebraic or even analytic.

For network analysis of microwave systems with time- and frequency-varying elements, the network can be broken down into block diagrams where the linear time- and frequency-varying element is isolated from the rest of the LFI or LTI components. This approach requires operational methods of combining the general linear element with other components, in cascade and parallel, to determine the overall system function. All linear devices (shift-invariant or not) can be combined in parallel by adding either their impulse response functions or (equivalently) their transfer functions [26]. For devices in series, however, determination of the combined response is not trivial, unless the devices are shift invariant. For example, the overall transfer function of LTI devices in series is accomplished by multiplying the individual transfer functions

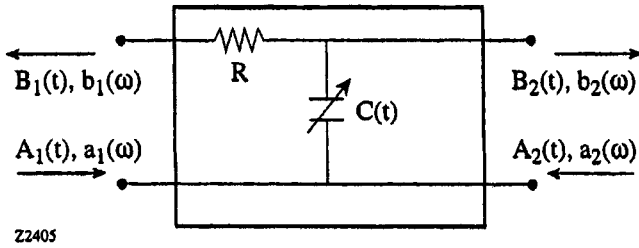


Fig. 1. Example of a linear device with a time-varying capacitance and, therefore, time-varying pole location (bandwidth). The time-varying frequency response cannot be completely characterized by a filter or modulator model.

together, or equivalently convolving their impulse responses. For LFI devices in series, the transfer (modulation) functions are multiplied while the spectral transform of the modulation is convolved.

To derive the transfer function of general linear devices in series, we begin with the repeated operation of the transfer function (in operational form)

$$\tilde{S}(p, t)[a(\omega)] = \tilde{S}_b(p, t) \left\{ \tilde{S}_a(p, t)[a(\omega)] \right\} \quad (8)$$

where $\tilde{S}_a(p, t)$ and $\tilde{S}_b(p, t)$ are the transfer functions for the first and second devices, respectively. $\tilde{S}_a(p, t)$ operates on $a(\omega)$, giving the product $\tilde{S}_a(\omega, t)a(\omega)$, and then by the product rule, $\tilde{S}_b(p, t)$ operates on both $\tilde{S}_a(\omega, t)$ and $a(\omega)$; the result being

$$\begin{aligned} \tilde{S}e^{j\omega t} &= \tilde{S}_b \left[e^{j\omega t} \frac{\partial}{\partial t} \tilde{S}_a + \tilde{S}_a \frac{\partial}{\partial t} e^{j\omega t} \right] \\ &= S_b e^{j\omega t} \frac{\partial}{\partial t} \tilde{S}_a + \tilde{S}_b j\omega e^{j\omega t} \tilde{S}_a. \end{aligned} \quad (9)$$

By simplifying (9), we find the transfer functional form of two linear devices in series as

$$\tilde{S}(p, t)A(t) = \tilde{S}_b(p + \omega, t) \left[\tilde{S}_a(p, t)A(t) \right]. \quad (10)$$

Therefore, by using the definition of (3), the combined transfer function of two general linear devices in series does not reduce to convolution or multiplication.

III. ANALYTICAL EXAMPLE

To demonstrate the application of the $\tilde{S}(\omega, t)$ system function to microwave device characterization, a simple lumped-element time- and frequency-varying device model will be solved analytically. The model, which is shown in Fig. 1, is a single-pole low-pass filter with a sinusoidally varying capacitive element $C(t) = C_0 + C_m \sin(\omega_m t)$.

The differential equation for this device can be written in the form of (1) as

$$\begin{aligned} A(t) &= \left[\frac{1}{2}C(t)(R + Z_0) \right] \frac{d}{dt} B(t) \\ &+ \left[1 + \frac{1}{2}R/Z_0 + \frac{1}{2}(R + Z_0) \frac{d}{dt} C(t) \right] B(t). \end{aligned} \quad (11)$$

From S -parameter analysis, the $S_{21}(\omega)$ for a conventional LTI filter (where $C(t) = C_0$ in Fig. 1) is given by

$$S_{21}(\omega) = \frac{2Z_0}{2Z_0 + R + j\omega C Z_0 (R + Z_0)}. \quad (12)$$

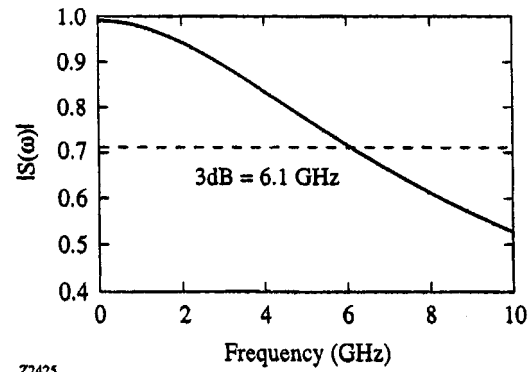


Fig. 2. Magnitude of the transfer function $S_{21}(\omega)$ of a low-pass single-pole filter, which is equivalent to the circuit in Fig. 1, but with a constant (unmodulated) capacitance.

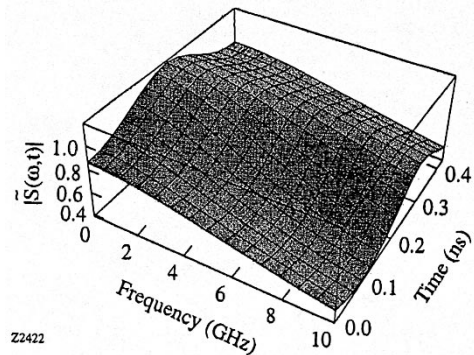


Fig. 3. Magnitude of the transfer function $\tilde{S}_{21}(\omega, t)$ of a low-pass single-pole filter with sinusoidally varying capacitance, plotted over one cycle of modulation and 150% of the bandwidth.

Applying (10) to the cascaded elements of resistance and shunt capacitance, we get

$$\tilde{S}_{21}(\omega, t) = \frac{2Z_0}{2Z_0 + R + (p + j\omega)C(t)Z_0 \cdot (R + Z_0)} \quad (13)$$

which also could have been found by the direct solution of the differential equation in (11). The $|\tilde{S}_{21}(\omega, t)|$ plot for the LTI version of this device is shown in Fig. 2, and $|\tilde{S}_{21}(\omega, t)|$ is shown in the elevation plot of Fig. 3 for one cycle of modulation. Observe that, in both figures, the low-pass attenuation is along the frequency axis. Also, Fig. 3 shows sinusoidal modulation of the frequency response along the temporal axis that shifts in phase for different frequencies.

Fig. 4 is a series of cross sections of Fig. 3 along the time axis, showing the modulating aspect of our model device, which is dependent on frequency. Fig. 5, a series of lineouts along the frequency axis, shows that, in our case, the low-pass filter shape depends on time. Although stability will not be considered in this paper, notice in both plots that the instantaneous magnitude of the transfer function can rise momentarily above unity, implying the possibility of device oscillation.

Later we will show windowed signals with surface density plots. Accordingly, for ease of comparison, here we will show a surface density plot of $\tilde{S}(\omega, t)$ in Fig. 6, plotted across several cycles of modulation in the time domain (along the vertical) and from in the frequency domain along the horizontal. For reference, Fig. 3, which is an elevation plot of $\tilde{S}(\omega, t)$ over one

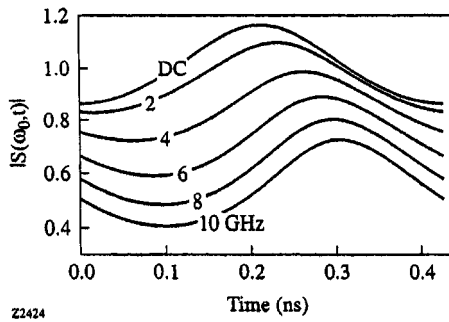


Fig. 4. Series of cross sections through $\tilde{S}_{21}(\omega, t)$ along the time axis, showing the change in the magnitude and phase of the modulation for different signal frequencies.

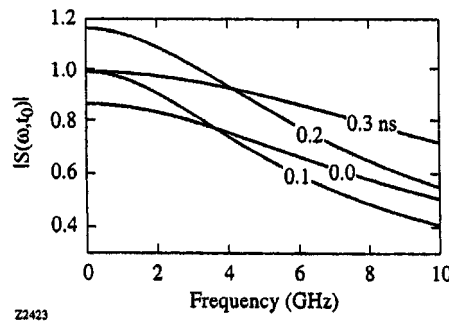


Fig. 5. Series of cross sections through $\tilde{S}_{21}(\omega, t)$ along the frequency axis, showing the change in instantaneous bandwidth for different times.

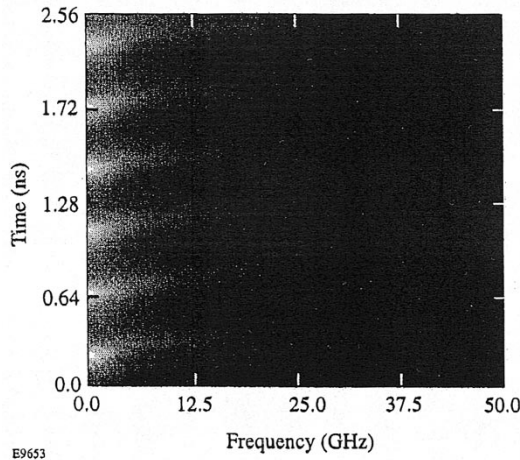


Fig. 6. Surface density plot of $|\tilde{S}_{21}(\omega, t)|$ with six cycles of modulation along the time axis and demonstrating low-pass filtering along the frequency axis.

modulation cycle and a smaller frequency span, covers the lower left-hand-side corner of this plot. Note that since we are modeling a single-pole low-pass filter, a $\pi/2$ phase shift occurs in $\tilde{S}(\omega, t)$ in the vicinity of the 3-dB frequency (i.e., the pole). This is seen in the surface density plot (Fig. 6) as a shift in the phase of the modulation versus frequency that occurs in the vicinity of the 3-dB frequency.

Using (6) and (13), we simulated the propagation of a sum of two sine waves through our model device. The attenuation and dispersion of each spectral component are demonstrated in Fig. 7, where the low-pass aspect is readily apparent. The influence of the modulation can best be compared by looking at a plot

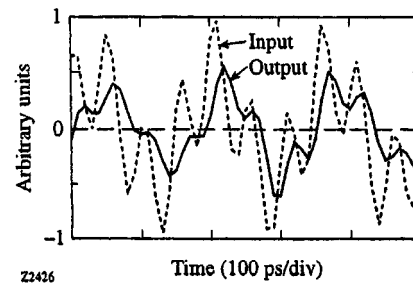


Fig. 7. Plot of input and output signals showing the DUTs low-pass filtering effect. The dashed line is the input signal, while the solid line is the output signal.

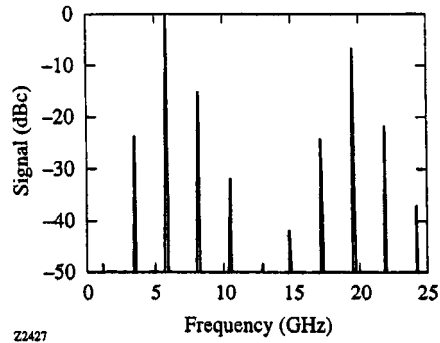


Fig. 8. Magnitude-only plot of the output-signal spectrum, showing changes in modulation characteristics for different frequencies.

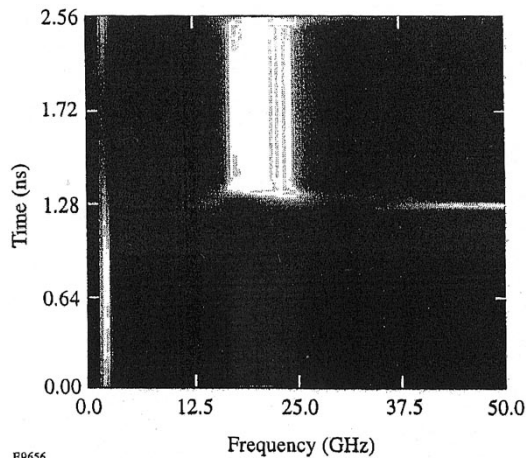
of the spectral output in Fig. 8, where the sinusoidal modulation adds differing sidebands to each input spectral component. Since this device not only modulates each frequency differently, but also filters the signals, standard network and spectrum analysis would not adequately characterize the device.

We will now attempt to use windowed signals to characterize our time-varying model filter by conventional S -parameter analysis, and we compare the results to the general $\tilde{S}(\omega, t)$ approach. To plot the windowed signals, we will use time-frequency distributions because they visually demonstrate the fundamental constraint due to the uncertainty principle; a narrow windowing in time necessarily leads to a broad frequency window and vice versa. This windowing dependency between the axes is easily observed on a time-frequency representation by the phenomenon of “minimum area”: a time-frequency distribution of a signal consists of areas (or regions) where the signal exists at a localized time and frequency. These areas cannot be smaller than a dimensionless constant (the product of time and frequency) determined by the uncertainty principle. This uncertainty is not a feature of time-frequency distributions, but of windowed signals in general; therefore, the choice of time-frequency distributions does not detract from the general demonstration of the uncertainty limitations of windowing.

To demonstrate the limitations of windowing, the particular choice of algorithm to generate a time-frequency representation is a matter of convenience. We will use

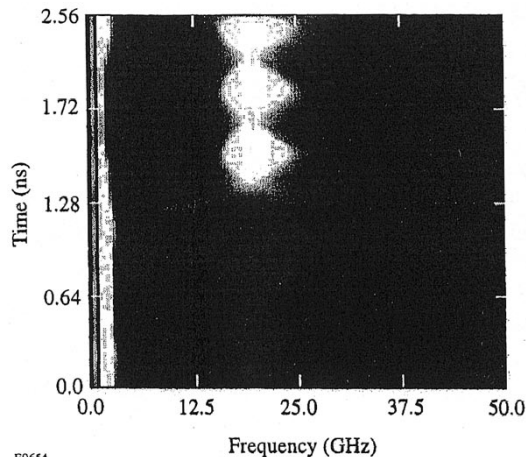
$$A(\omega; t) = \int_{-\infty}^{\infty} A(t)|\omega|e^{-j\omega^2(t-\tau)^2} d\tau \quad (14)$$

where $A(\omega; t)$ is the time-frequency distribution of $A(t)$ and a semicolon is used between the time-frequency variables to



E9656

Fig. 9. Time-frequency representation (ambiguity function) of a 2-GHz sine wave that transitions abruptly to a 20-GHz sine wave. Due to window tradeoffs, low frequencies are smeared vertically and high frequencies are smeared horizontally. In addition, some wraparound from top to bottom is caused by the FFT algorithm.



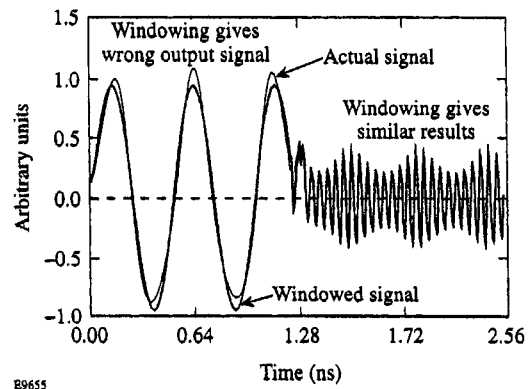
E9654

Fig. 10. Time-frequency representation of the output signal, after multiplication of the input time-frequency distribution with the system function $S_{21}(\omega, t)$. The effect of the system function is shown by the attenuation of the high-frequency signals and temporal ripple in the different spectral components.

emphasize the dependence of the axes. This definition has the virtues of showing all the essential features of time-frequency distributions and being easily transformable back into the Fourier transform of the signal by integration

$$a(\omega) = \int_{-\infty}^{\infty} A(\omega; t) dt. \quad (15)$$

Fig. 9 shows an example time-frequency representation of a signal to be propagated through our model filter: low-frequency sine wave that abruptly transitions (with broad-band noise) to a higher-frequency sine wave. It is easy to see the smearing of the signal in time (for the low frequencies) and frequency (for the high frequencies) caused by fundamental windowing tradeoffs. Although the fast Fourier transform (FFT) algorithm used to generate the plot causes “leaking” across the boundary of the plot, these artifacts have no impact on the results.



E9655

Fig. 11. Time-domain comparison of output signals using the technique described in this paper (dashed line) and the windowing method (solid line). Windowing can be applied successfully to the high-frequency segment of the signal where the modulation is slow compared to the cycle; however, it averages over the system function for the first segment.

By multiplying the input signal $A(\omega; t)$ of Fig. 9 with the system function $\tilde{S}(\omega, t)$ of Fig. 6, the time-frequency representation of the output signal shown in Fig. 10 results. Important features of the output signal are the low-pass filtering (shown clearly in Fig. 10 in the spectral content of the transition noise) and the differences in modulation of each spectral component, both in amplitude and phase.

Converting back to the frequency domain using (15) and then inverse Fourier transforming to the temporal signal, we can compare the windowed output signal with the one based on the $\tilde{S}(\omega, t)$ technique. The windowed method is represented by the thick line in Fig. 11, while the \tilde{S} result is the thin line. It is evident that the windowing approach produced acceptable results for the second half of the signal, when the modulation was much slower than the signal (i.e., the slowly varying envelope approximation was valid). For the first half, the modulation was comparable to the signal frequency, and the “window” effectively smeared the amplitude and phase modulation in time. Choosing a narrower time window would not solve the fundamental problem since doing so would automatically broaden the spectral window, causing increased smearing of the spectral response.

IV. CONCLUSIONS

When a linear microwave device, such as a photoconductive switch, has rapid changes both in its temporal and spectral responses, and the temporal variations cannot be controlled independently (i.e., cannot be made separable for the analysis purposes), standard windowed S -parameters cannot be applied accurately. To allow characterization of such devices, we developed a linear system function $\tilde{S}(\omega, t)$. We presented the most important properties of the \tilde{S} -parameter and showed similarities to the conventional S -parameter analysis that preserve most features of the Fourier transform tables. The transfer function of a simple linear time-varying device was calculated and analyzed. Also, an example signal was propagated through the device, using our \tilde{S} transfer function. To demonstrate the limitations of windowing, we applied the windowed (time-frequency) representation of an input signal to \tilde{S} . Due to the uncertainty

principle, which causes a tradeoff between temporal and spectral window resolutions, the resulting output signal was unable to follow both time and spectral variations in the device.

Photoconductive microwave semiconductor devices are an example of practical devices that can operate in a regime that requires the generalized transfer function $\tilde{S}(\omega, t)$ for complete characterization and optimization. The carrier dynamics of photoconductive devices occur on the time scales of microwave and millimeter-wave signals. Since the carrier population distribution can affect the microwave transmission of the device, the scattering parameters can vary on the time scale of the applied signal. To measure $\tilde{S}(\omega, t)$ of a photoconductive microwave switch, one could illuminate the switch and repeatedly apply a series of single-frequency signals, then measure the instantaneous amplitude and phase of each output signal as it evolves over time. A lumped-element model of the switch can then be fitted to \tilde{S} , and by relating physical switch properties such as gap length, contact resistance, and capacitance to the lumped elements, a suitable route to switch optimization can be determined. A detailed description of this optimization will be described in a separate paper.

ACKNOWLEDGMENT

The authors thank M. Wengler, Qualcomm, San Diego, CA, for critical reading of this paper's manuscript and very insightful comments.

REFERENCES

- [1] R. Achar and M. S. Nakhla, "Efficient transient simulation of embedded subnetworks characterized by S -parameters in the presence of nonlinear elements," *IEEE Trans. Microwave Theory Tech.*, vol. MTT-46, pp. 2356–2363, Dec. 1998.
- [2] C. W. Hsue and C. D. Hechtman, "Transient responses of an exponential transmission line and its applications to high-speed backdriving in in-circuit test," *IEEE Trans. Microwave Theory Tech.*, vol. 42, pp. 458–462, Mar. 1994.
- [3] L. A. Hayden and V. K. Tripathi, "Nonuniformly coupled microstrip transversal filters for analog signal-processing," *IEEE Trans. Microwave Theory Tech.*, vol. 39, pp. 47–53, Jan. 1991.
- [4] A. H. Mohammadian and C. T. Tai, "A general method of transient analysis for lossless transmission lines and its analytical solution to time-varying resistive terminations," *IEEE Trans. Antennas Propagat.*, vol. AP-32, pp. 309–312, Mar. 1984.
- [5] A. R. Djordjevic, T. K. Sarkar, and R. F. Harrington, "Analysis of lossy transmission-lines with arbitrary nonlinear terminal networks," *IEEE Trans. Microwave Theory Tech.*, vol. MTT-34, pp. 660–666, June 1986.
- [6] J. E. Schutt-Aine and R. Mittra, "Scattering parameter transient analysis of transmission lines loaded with nonlinear terminations," *IEEE Trans. Microwave Theory Tech.*, vol. 36, pp. 529–536, Mar. 1988.
- [7] J. E. Schutt-Aine, "Transient analysis of nonuniform transmission lines," *IEEE Trans. Circuits Syst. I*, vol. 39, pp. 378–385, May 1992.
- [8] T. Dhaene, L. Martens, and D. Dezzutter, "Transient simulation of arbitrary nonuniform interconnection structures characterized by scattering parameters," *IEEE Trans. Circuits Syst. I*, vol. 39, pp. 928–937, Nov. 1992.
- [9] K. S. Oh and J. E. Schutt-Aine, "Transient analysis of coupled, tapered transmission lines with arbitrary nonlinear terminations," *IEEE Trans. Microwave Theory Tech.*, vol. 41, pp. 268–273, Feb. 1993.
- [10] B. Boyer, J. Haidar, A. Vilcot, and M. Bouthinon, "Tunable microwave load based on biased photoinduced plasma in silicon," *IEEE Trans. Microwave Theory Tech.*, vol. 45, pp. 1362–1367, Aug. 1997.
- [11] S. E. Saddow and C. H. Lee, "Optical control of microwave integrated circuits using high-speed GaAs and Si photoconductive switches," *IEEE Trans. Microwave Theory Tech.*, vol. 43, pp. 2414–2420, Sept. 1995.

- [12] A. A. De Salles, "Optical control of GaAs MESFET's," *IEEE Trans. Microwave Theory Tech.*, vol. MTT-31, pp. 812–820, Oct. 1983.
- [13] J. L. Gautier, D. Pasquet, and P. Pouvil, "Optical effects on the static and dynamic characteristics of a GaAs MESFET," *IEEE Trans. Microwave Theory Tech.*, vol. MTT-33, pp. 819–822, Sept. 1985.
- [14] I. L. Andersson and S. T. Eng, "Phase and amplitude characteristics of InP:Fe modified interdigitated gap photoconductive microwave switches," *IEEE Trans. Microwave Theory Tech.*, vol. 37, pp. 729–733, Apr. 1989.
- [15] L. E. M. de Barros, Jr., A. Paoletta, M. Y. Frankel, M. A. Romero, P. R. Herczfeld, and A. Madjar, "Photoresponse of microwave transistors to high-frequency modulated lightwave carrier signal," *IEEE Trans. Microwave Theory Tech.*, vol. 45, pp. 1368–1374, Aug. 1997.
- [16] G. W. Wornell, "Emerging applications of multirate signal processing and wavelets in digital communications," *Proc. IEEE*, vol. 84, pp. 586–603, Apr. 1996.
- [17] B.-S. Chen, Y.-C. Chung, and D.-F. Huang, "Optimal time–frequency deconvolution filter design for nonstationary signal transmission through a fading channel: AF filter bank approach," *IEEE Trans. Signal Processing*, vol. 46, pp. 3220–3224, Dec. 1998.
- [18] H.-N. Lee and G. J. Pottie, "Fast adaptive equalization/diversity combining for time-varying dispersive channels," *IEEE Trans. Commun.*, vol. 46, pp. 1146–1162, Sept. 1998.
- [19] L. M. Silverman, "Realization of linear dynamical systems," *IEEE Trans. Automat. Contr.*, vol. AC-16, pp. 554–567, June 1971.
- [20] G. H. Owyang, *Foundations for Microwave Circuits*. Berlin, Germany: Springer-Verlag, 1989.
- [21] H. D'Angelo, *Linear Time-Varying Systems: Analysis and Synthesis*, ser. Electrical Engineering. Boston, MA: Allyn & Bacon, 1970.
- [22] B. Boashash, "Estimating and interpreting the instantaneous frequency of a signal I: Fundamentals," *Proc. IEEE*, vol. 80, pp. 520–538, Apr. 1992.
- [23] H. N. Kritikos and J. G. Teti, "A time–frequency analysis method for radar scattering," *IEEE Trans. Microwave Theory Tech.*, vol. 46, pp. 257–260, Mar. 1998.
- [24] S. R. Kunasani and C. Nguyenj, "Distortion of pulsed signals in microstrip transmission lines using short-time Fourier transform," *IEEE Microwave Guided Wave Lett.*, vol. 6, pp. 1–3, Jan. 1996.
- [25] H. Ling, J. Moore, D. Bouche, and V. Saavedra, "Time–frequency analysis of backscattered data from a coated strip with a gap," *IEEE Trans. Antennas Propagat.*, vol. 41, pp. 1147–1150, Aug. 1993.
- [26] W. Kaplan, *Operational Methods for Linear Systems*, ser. Mathematics. Reading, MA: Addison-Wesley, 1962.

Kenton Green (S'91–M'99) received the B.S. degree in electrical engineering from the University of Houston, Houston, TX, in 1992, and the M.S. and Ph.D. degrees in electrical engineering from the University of Rochester, Rochester, NY, in 1995 and 1999, respectively.

He is currently with the University of Rochester. His research interests include photoconductive microwave devices and nonlinear optics.

Dr. Green is a member of the IEEE Lasers and Electro-Optics Society (IEEE LEOS) and the Optical Society of America (OSA).

Roman Sobolewski (M'98) received the M.S. degree in electrical engineering from the Warsaw Technical University, Warsaw, Poland, in 1975, and the Ph.D. and Sc.D. degrees in physics from the Polish Academy of Sciences, Warsaw, Poland, in 1983 and 1992, respectively.

He is currently a Senior Scientist in the Laboratory for Laser Energetics, with a joint appointment as a Senior Scientist and Professor in the Department of Electrical and Computer Engineering, University of Rochester, Rochester, NY. His research interests include ultrafast phenomena in solids, new device concepts for high-performance ultrafast optoelectronics and electronics, time-domain scanning tunneling spectroscopy, digital superconducting electronics, femtosecond laser sources, as well as the nonequilibrium superconductivity and fabrication and electronic and optoelectronic properties of high-temperature superconducting materials and devices.

Dr. Sobolewski is a member of the International Society for Optical Engineering (SPIE). He is also the chair of the Rochester Chapter of the IEEE Electrical Devices Society.